

Performance Improvement of a ZnGa_2O_4 Extended-Gate Field-Effect Transistor pH Sensor

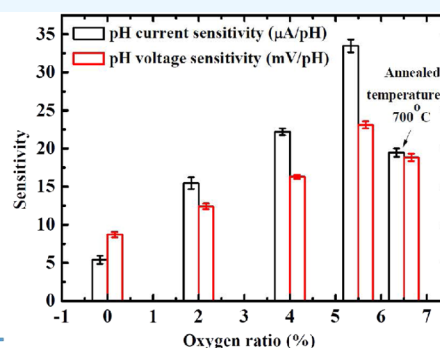
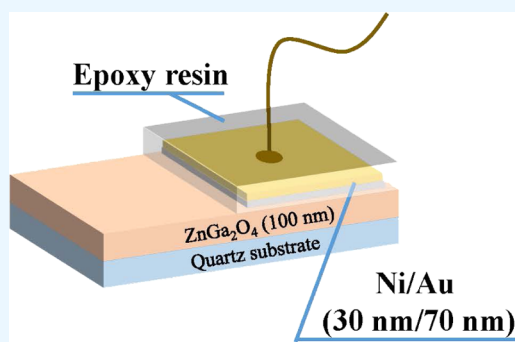
Chia-Hsun Chen,^{||} Shu-Bai Liu,^{||} and Sheng-Po Chang^{*||}Cite This: *ACS Omega* 2024, 9, 15304–15310

Read Online

ACCESS |

Metrics & More

Article Recommendations



ABSTRACT: ZnGa_2O_4 sensing films were prepared using an RF magnetron sputtering system and connected to a commercial metal oxide semiconductor field-effect transistor (MOSFET) as the extended-gate field-effect transistor (EGFET) to detect pH values. Experimental parameters were adjusted by varying the oxygen flow rate in the process chamber to produce ZnGa_2O_4 sensing films with different oxygen ratios. These films were then treated in a furnace tube at an annealing temperature of 700 °C. The sensitivity and linearity of the constant current mode and the constant voltage mode were measured and analyzed in the pH range of 2–12. Under the deposition conditions with an oxygen ratio of 6%, the sensitivity reached 23.14 mV/pH and 33.49 $\mu\text{A}/\text{pH}$, with corresponding linearity values of 92.1 and 96.15%, respectively. Finally, the sensing performance of the ZnGa_2O_4 EGFET pH sensor with and without annealing processes was analyzed and compared.

INTRODUCTION

In recent years, pH sensors have garnered significant interest across various fields, such as chemical and biological applications,¹ clinical detection,² and environmental analysis.³ Continuous monitoring of health conditions is of paramount importance, with applications ranging from early diagnosis, including noninvasive glucose monitoring with contact lenses,⁴ to pH value detection on tooth surfaces for caries diagnosis.^{5,6} In pursuit of these diverse sensing applications, various materials, including silicon nitride (Si_3N_4),⁷ titanium oxide (TiO_2),⁸ and zinc oxide (ZnO),⁹ have been employed and fabricated as sensing films for detecting H^+ and OH^- ions. However, among these materials, the wide-band-gap material ZnGa_2O_4 , introduced in this work, offers several distinct advantages. Notably, it exhibits high chemical stability and functions as a transparent conducting oxide in the ultraviolet (UV) region, effectively mitigating the effects of light and temperature.^{10,11} In particular, ZnGa_2O_4 displays excellent faradaic efficiency properties, a quality that has been verified and documented in the previous literature.^{12,13} Consequently, ZnGa_2O_4 has attracted significant attention as a promising material for constructing sensing films for EGFET pH sensors. Earlier research explored various methods for pH value

measurement. Typically, glass sensing electrodes were widely used to measure hydrogen ion concentrations and displayed favorable measurement characteristics. However, glass electrodes have certain drawbacks, such as fragility, the need for constant wet storage, and limitations in miniaturization, greatly limiting their practical applications.¹⁴ To address these shortcomings, Piet Berveld introduced the concept of an ion-sensitive field-effect transistor (ISFET) based on the MOSFET in 1970.¹⁵ This adaptation involved replacing the traditional metal component of the MOSFET with a layer of metal oxide sensing films. When the sensing film of the ISFET is immersed in a solution, it generates an interface potential that varies with changes in the ion concentration within the solution. These ion concentration variations affect the current–voltage characteristics of the field-effect transistor (FET). The

Received: December 13, 2023

Revised: March 3, 2024

Accepted: March 6, 2024

Published: March 20, 2024



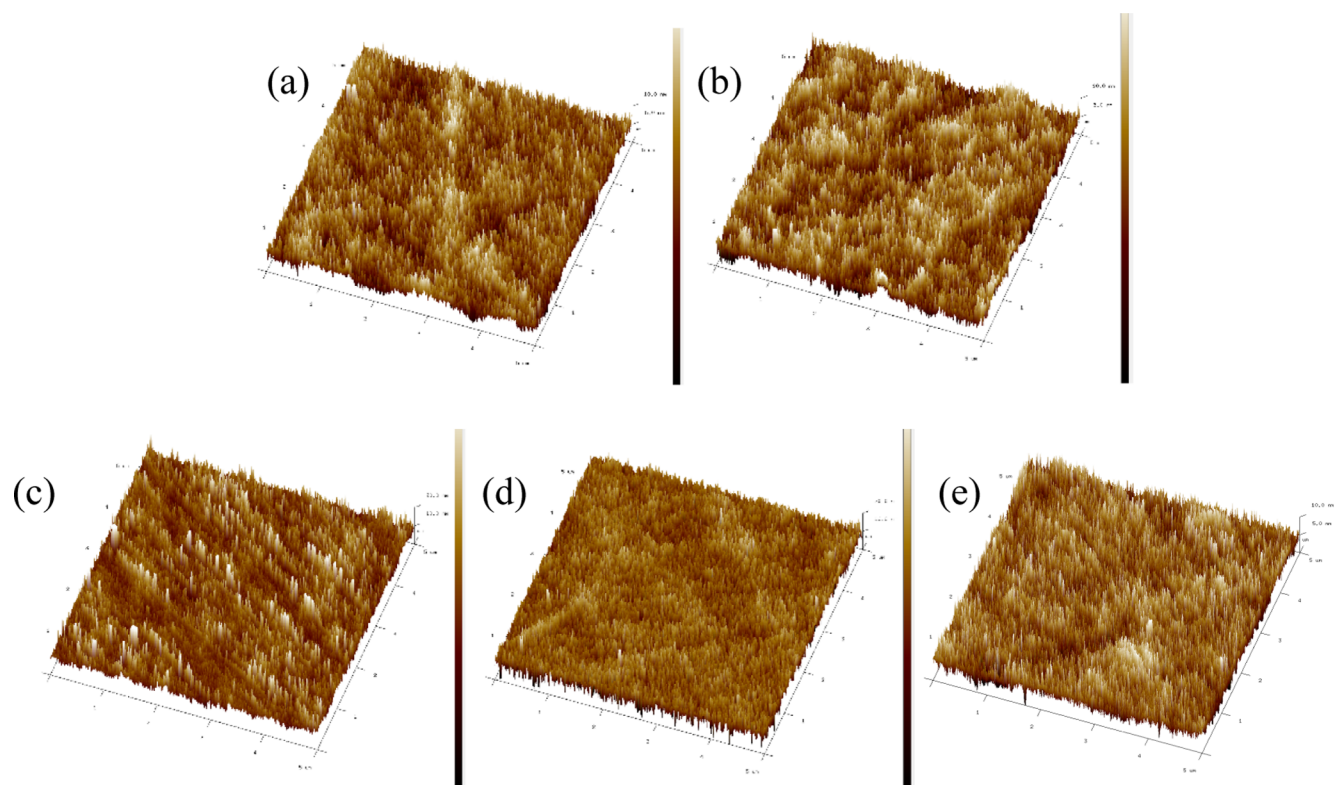


Figure 1. AFM images of the surface morphology of ZnGa_2O_4 sensing films under different oxygen flow ratios of (a) 0%, (b) 2%, (c) 4%, (d) 6%, and (e) 6% with an annealing temperature of 700 °C, respectively.

ISFET offers numerous advantages, including a fast response time for real-time measurements, potential for miniaturization, and compatibility with the MOSFET process, which significantly reduces production costs. As a result, pH sensing using the ISFET structure has become a more favorable approach compared to traditional glass electrodes.¹⁶ However, ISFET technology is not without its challenges, including issues of instability, susceptibility to electrostatic discharge (ESD) damage, and the presence of a leakage current. In order to enhance the properties of ISFET and mitigate associated risks, Spiegel et al. introduced the EGFET in 1983.¹⁷ The EGFET structure effectively separates the sensing film from the FET while retaining the metal gate of the FET. In essence, the EGFET consists of two distinct components: the sensing film and the MOSFET, connected by wires. Furthermore, when compared with ISFET and other methods such as biofluid and interstitial fluid (ISF), EGFETs offer several key advantages. These include a separated structure that shields the MOSFET components from the solution, ensuring long-term stability, insensitivity to light and temperature, ease of packaging, cost-effectiveness, simplicity, and the absence of microneedles (MN).^{18–21} For these reasons, the EGFET structure was chosen for this study and connected to ZnGa_2O_4 sensing films to detect pH values. It not only has the advantage of the above reason but could also be quickly analyzed by the sensing platforms of the EGFET structure and could quickly obtain the performance of the ZnGa_2O_4 sensing films. The material characteristics of the ZnGa_2O_4 sensing films were thoroughly examined by using atomic force microscopy (AFM) and X-ray diffraction (XRD). Additionally, the electrical properties were measured and analyzed in both the constant current and constant voltage modes to determine pH voltage sensitivity and pH current sensitivity, respectively.

RESULTS AND DISCUSSION

When a sensing film is immersed in an electrolyte solution, the reaction between the film and the solution is primarily determined by the surface properties. The film's surface is characterized by numerous metal–OH bonds formed by dangling bonds. According to the site binding model, the metal–OH groups can accept or donate a proton and make the surface charge accrete. When the sensing film is immersed in an acidic solution (lower pH value), the high accretion of H^+ ions on the sensing film provides a positive charge (OH_2^+). On the contrary, when the sensing film is immersed in an alkali solution (higher pH value), the high accretion of OH^- ions on the sensing film provides a negative charge (O^-). The mechanism is known as “protonation” and “deprotonation”, which results in a change in surface potential as the sensing film is immersed in solutions with different pH values. Therefore, the surface characteristics of the sensing film are very important for the sensing performance. Next, the surface characteristics of the ZnGa_2O_4 sensing film and the I–V transfer characteristics of the ZnGa_2O_4 EGFET pH sensor with various oxygen ratios were discussed.

The surface morphology of the ZnGa_2O_4 thin film with various oxygen flow ratios was characterized using atomic force microscopy (AFM) with a scanning area of $5\ \mu\text{m} \times 5\ \mu\text{m}$. Figure 1a–d presents the AFM images of the ZnGa_2O_4 sensing films with varying oxygen flow ratios. Specifically, the ZnGa_2O_4 sensing films with oxygen flow ratios of 0, 2, 4, and 6% exhibited root-mean-square (RMS) roughness values of 1.31, 1.55, 2.19, and 2.58 nm, respectively. It is evident that the root-mean-square (RMS) roughness increased as the oxygen flow ratio was raised. To further realize the effect of the annealing process, the ZnGa_2O_4 sensing films with oxygen flow ratios of

6% were annealed at a temperature of 700 °C, and a root-mean-square (RMS) roughness of 1.49 was measured, as shown in Figure 7e.

To assess the performance of the ZnGa₂O₄ EGFET pH sensor, we discuss the transfer characteristics and transconductance curves obtained under the constant current mode. The ZnGa₂O₄ EGFET pH sensor operated in the linear region with a fixed drain voltage (V_{DS}) of 0.2 V, while the measured reference voltage (V_{REF}) was varied from 0 to 3 V. Figure 2

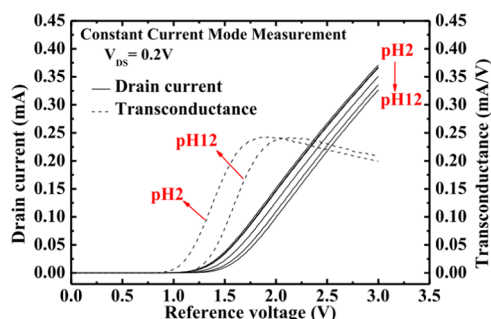


Figure 2. I_{DS} – V_{REF} transfer characteristics and transconductance curves of the ZnGa₂O₄ EGFET pH sensor with an oxygen flow ratio of 6%.

shows the transfer characteristics and transconductance curves of the ZnGa₂O₄ EGFET pH sensor with an oxygen flow ratio of 6%. As shown in Figure 2, the peak values of the transconductance curves within the pH range of 2–12 remain consistent, indicating that temperature effects can be considered negligible.²² As a result in Figure 2, the curves of the transconductance shifted to a positive reference voltage with increasing pH values from 2 to 12 owing to the surface reaction of protonation and deprotonation. Based on the MOSFET theory, the relationship between drain current (I_{DS}) and reference voltage (V_{REF}), while operating in the linear region of the ZnGa₂O₄ EGFET pH sensor, can be described by the following equation^{23,24}

$$I_{DS} = \frac{\mu_n C_{ox}}{2} \left(\frac{W}{L} \right) [2(V_{REF} - V_{T,EGFET})V_{DS} - V_{DS}^2] \quad (1)$$

where μ_n is the carrier mobility of the channel, C_{ox} is the gate oxide capacitance per unit area, W is the channel width, L is the channel length, V_{REF} is the voltage of the applied voltage of the reference electrode, $V_{T,EGFET}$ is the threshold voltage of the EGFET, and V_{DS} is the drain to source voltage. In the expression formula of I_{DS} , $V_{T,EGFET}$ was affected by different pH values when the ZnGa₂O₄ sensing film was immersed in the buffer solution. $V_{T,EGFET}$ could be defined and expressed by the following equation^{25,26}

$$V_{T,EGFET} = V_{T,MOSFET} - \frac{\varphi_M}{q} - E_{REF} + \chi^{sol} - \phi \quad (2)$$

where $V_{T,MOSFET}$ is the threshold voltage of the MOSFET, φ_M is the metal gate work function of the reference electrode, q is the electron charge, E_{REF} is the potential of the reference, χ^{sol} is the surface dipole potential of the electrolytic solution, and ϕ is the surface potential between the interface of the pH buffer solution and the ZnGa₂O₄ sensing films. The surface potential (ϕ) that depended on the pH value of the electrolyte could be expressed by the following equation^{27,28}

$$2.303(\text{pH}_{pzc} - \text{pH}) = \frac{q\phi}{KT} + \sin h^{-1} \left(\frac{q\phi}{KT\beta} \right) \quad (3)$$

where pH_{pzc} is the pH value of the buffer solution at the point of zero charge, K is Boltzmann's constant, T is the absolute temperature, and β is the parameter of the sensitivity. Based on the site binding model of the electrical double layer,²⁹ the parameter of the sensitivity (β) could be evaluated by using the following equation^{27,28}

$$\beta = \frac{2q^2 N_s \sqrt{K_b/K_a}}{KTC_{DL}} \quad (4)$$

where N_s is the surface sites per unit area, C_{DL} is the capacitance of the electrical double layer, K_a is the equilibrium constant of acid, and K_b is the equilibrium constant of the base. According to the theory described above, $V_{T,EGFET}$ is influenced by different pH values and is further affected by the surface potential (ϕ), resulting in varying drain currents (I_{DS}) obtained in different pH buffer solutions. Therefore, the transfer characteristic curve (I_{DS} – V_{REF}) in Figure 2 exhibits a right shift in the threshold voltage as the pH value increases, which is a result of the decreasing concentration of hydrogen ions. The drain current output characteristics in the saturation region of the ZnGa₂O₄ extended-gate field-effect transistor pH sensor could be expressed as follows.^{28,30}

$$I_{DS} = \frac{\mu_n C_{ox}}{2} \left(\frac{W}{L} \right) [(V_{REF} - V_{T,EGFET})^2] \quad (5)$$

It was observed that the drain current in the saturation region depended on the pH value and decreased with an increasing pH value. Figure 3 shows that higher pH values in

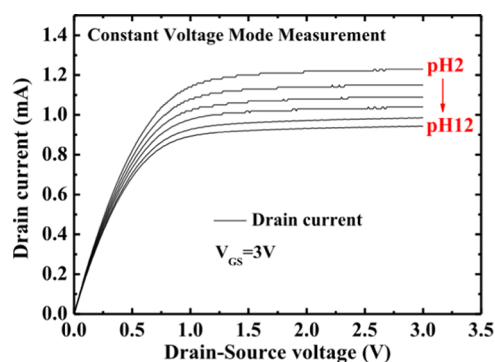


Figure 3. ZnGa₂O₄ extended-gate field-effect transistor pH sensor analyzed by the method of constant voltage mode measurement.

the pH buffer solution result in a lower drain current, primarily because a larger pH value implies a lower concentration of H⁺ ions in the pH buffer solution. The decreased concentration of H⁺ ions leads to changes in the ZnGa₂O₄ sensing films' surface potential, resulting in a negative voltage being applied to the ZnGa₂O₄ EGFET pH sensor. Consequently, the drain current decreases with increasing pH values.

The pH sensitivity refers to the voltage or current changes caused by variations in the pH levels. The pH sensitivity of the ZnGa₂O₄ thin-film EGFET pH sensor can be determined from the I_D – V_{REF} and I_D – V_{DS} transfer characteristics curve, covering a pH range from 2 to 12, using a first-order linear equation. Once the linear equation is identified, the sensitivity can be extracted from the slope and linearity is obtained, too.

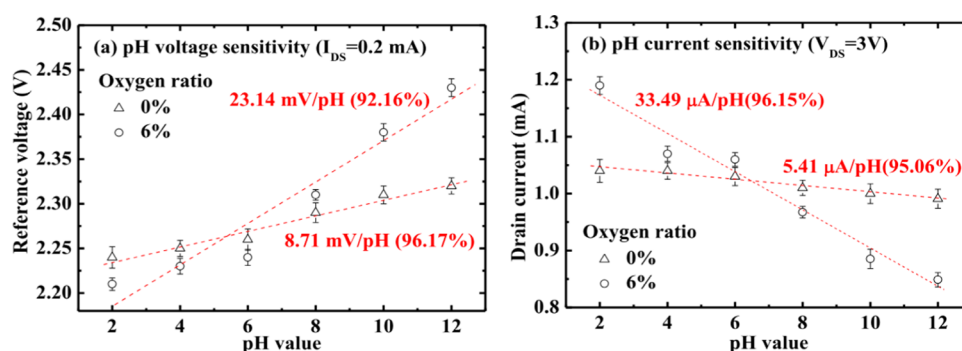


Figure 4. Sensitivity and linearity of the ZnGa_2O_4 extended-gate field-effect transistor pH sensor of (a) pH voltage sensitivity and (b) pH current sensitivity.

To assess the sensitivity and linearity of the ZnGa_2O_4 EGFET pH sensor, the performance of both the linear and saturation regions is depicted in Figure 4a,b, respectively. In the linear region, the pH voltage sensitivity and linearity were assessed and fitted based on the measured results obtained in the constant current mode, with the drain current fixed at 0.2 mA. The corresponding reference voltage was then plotted in Figure 4a and used to calculate the sensitivity. Therefore, the sensitivity of the linear region can be calculated using the following equation²⁶

$$\text{pH voltage sensitivity} = \frac{\Delta V_{T,\text{EGFET}}}{\Delta \text{pH}}$$

where ΔpH represents the pH difference of the electrolyte and $\Delta V_{T,\text{EGFET}}$ represents the variation of the threshold voltage of EGFET corresponding to the pH value difference.

As shown in Figure 4a, the pH voltage sensitivity for oxygen ratios of 0 and 6% was found to be 8.71 and 23.14 mV/pH, respectively. The corresponding linearity for oxygen ratios of 0 and 6% stood at 96.17 and 92.16%, respectively. This indicates that the pH voltage sensitivity for an oxygen ratio of 6% exceeded that of the oxygen ratio of 0%. Additionally, evaluating device characteristics operating in the saturation region under a fixed V_{DS} of 3 V was crucial for assessing the pH current sensitivity. The pH current sensitivity is shown in Figure 4b and could be calculated using the following equation³¹

$$\text{pH current sensitivity} = \frac{\Delta I_{DS}}{\Delta \text{pH}}$$

where ΔpH represents the pH difference of the electrolyte and ΔI_{DS} represents the variation of the drain current corresponding to the pH value difference.

As shown in Figure 4b, the pH current sensitivity for the ZnGa_2O_4 sensing films with an oxygen ratio of 6% was 33.49 μ A/pH, with a fitted linearity of 96.15%. In comparison to the ZnGa_2O_4 sensing films with an oxygen ratio of 0%, it is evident that the ZnGa_2O_4 sensing films with an oxygen ratio of 6% exhibited a higher root-mean-square (RMS) roughness, providing more surface binding sites and a larger effective sensing area.

The pH voltage sensitivity and pH current sensitivity of ZnGa_2O_4 sensing films with various oxygen flow ratios are presented in Figure 5. As observed in Figure 5, the pH sensing performance of ZnGa_2O_4 EGFET pH sensors, in terms of pH voltage sensitivity and pH current sensitivity, both exhibited variations with different oxygen flow ratios. Specifically, when

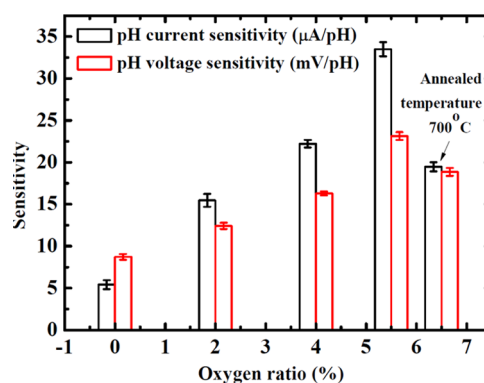


Figure 5. pH voltage sensitivity and pH current sensitivity of ZnGa_2O_4 films with various oxygen flow ratios.

compared with the pH voltage sensitivity of 8.71 mV/pH with an oxygen ratio of 0%, the pH voltage sensitivity improved with increasing oxygen ratios. The pH voltage sensitivities for oxygen ratios of 2, 4, and 6% were measured at 12.43, 16.29, and 23.14 mV/pH, respectively. Furthermore, the pH current sensitivity for an oxygen flow ratio of 0% was 5.41 μ A/pH and increased with the rise in the oxygen flow ratio. The corresponding pH current sensitivities for oxygen ratios of 2, 4, and 6% were measured at 15.46, 22.22, and 33.49 μ A/pH, respectively. Both pH voltage sensitivity and pH current sensitivity improved as the oxygen ratio increased. According to the site binding model theory,²⁹ with an increase in the oxygen flow rate, the root-mean-square (RMS) surface roughness became higher. This higher surface roughness suggests a greater surface contact area available for the reaction with the pH buffer solution. Consequently, this leads to improved reaction efficiency at the interface between the pH buffer solution and ZnGa_2O_4 sensing films. Ultimately, this results in more significant changes in surface potential as the pH value varies, particularly under the conditions of a 6% oxygen ratio. To further assess the impact of crystallinity on sensing performance, a ZnGa_2O_4 extended-gate field-effect transistor pH sensor was manufactured and subjected to annealing at a temperature of 700 °C.

X-ray diffraction (XRD) was employed to measure and characterize the lattice characteristics. Figure 6 presents the X-ray diffraction (XRD) curve for the ZnGa_2O_4 sensing films with an oxygen ratio of 6%, both without annealing and after annealing at 700 °C. As shown in Figure 6, the as-deposited ZnGa_2O_4 exhibits no regular arrangement of atoms, and no discernible peaks indicative of an amorphous structure are

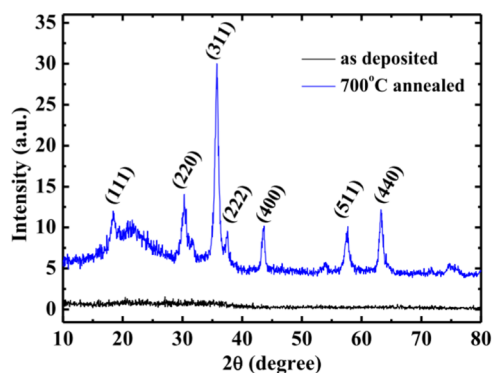


Figure 6. XRD spectra of ZnGa_2O_4 films with and without an annealing process.

observed. This observation is consistent with the results reported in the previous literature.³² However, following annealing at a temperature of 700 °C, the films underwent crystallization and exhibited a polycrystalline phase. Notably, the diffraction peaks were observed near 35.90, 37.35, 57.60, and 63.75°, corresponding to the (311), (222), (511), and (440) planes of ZnGa_2O_4 , respectively (JCPDS card 381240), indicative of a spinel structure. These peaks closely align with 35.73, 37.37, 57.45, and 63.10°, respectively.³³ The pH current sensitivity and pH voltage sensitivity are also shown in Figure 5. It is evident that the pH current sensitivity and pH voltage sensitivity, when using an oxygen ratio of 6% under annealing at 700 °C, were measured at 19.48 $\mu\text{A}/\text{pH}$ and 18.86 mV/pH, respectively. However, a comparison with the results obtained without the annealing process reveals that the sensitivity was smaller with the annealing temperature set at 700 °C. This difference can be attributed to the significant impact of the surface passivation process resulting from the annealing temperature of 700 °C, leading to a phase transition from the amorphous phase to the crystalline phase, as demonstrated in Figure 6. Furthermore, with an annealing temperature of 700 °C, the crystallization of the material became more distinct and the full width at half-maximum (fwhm) narrowed, signifying higher film quality. While the thin film quality could be enhanced through the annealing process, it did not lead to improved sensitivity performance. This lack of improvement can be attributed to the reduction in surface site density, which hinders the interaction between the solution and the ZnGa_2O_4 sensing films. To further illustrate the influence of the surface roughness and vacancies, ZnGa_2O_4 sensing films with a 6% oxygen flow ratio were annealed at a temperature of 700 °C. First, the root-mean-square (RMS) roughness decreased from 2.58 nm (as-deposited) to 1.49 nm (after annealing at 700 °C). Second, characterization using X-ray photoelectron spectroscopy (XPS) was carried out, where the O_{II} peak area to the total peak area of O_{Is} was defined to compare oxygen deficiency in the various films. The higher O_{II} ratio correlated with more vacancies in the films. The relative proportions of the O_{II}/O_{Is} ratio decreased from 57.64% (unannealed) to 26.93% after annealing at 700 °C.³⁴ Therefore, both surface roughness and vacancies are crucial factors that need to be considered and analyzed.

In order to study the reliability of the ZnGa_2O_4 extended-gate field-effect transistor pH biosensor, a switch test was measured and revealed the real-time drain current of the loop with pH 2–12, as shown in in Figure 7. The switch test is based on the constant voltage mode measurement of V_{DS} and

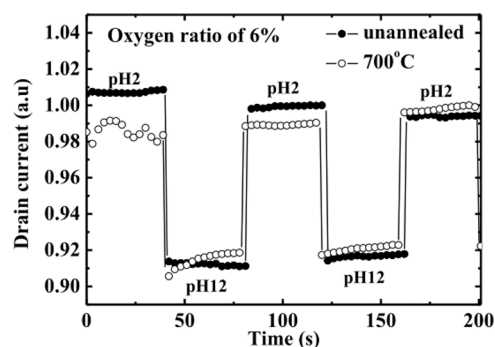


Figure 7. Switch test of the ZnGa_2O_4 extended-gate field-effect transistor pH biosensor unannealed and annealed at 700 °C.

V_{GS} operated at 3 V. When the current value changes suddenly, the drain current is recorded in the current time mode to monitor the change of the saturation current. As shown in Figure 7, it could be observed that the ZnGa_2O_4 sensing films have great response and corrosion resistance.

Table 1 shows the comparison of the pH sensing performance of various metal oxide materials published in the previous literature. As shown in Table 1, the pH voltage sensitivity of ZnO pH sensors ranged from 15.4 to 24.67 mV/pH, whereas InN and CuO exhibited 22.66 and 18.4 mV/pH, respectively.^{35–38} Compared to the above results, the ZnGa_2O_4 pH sensor studied in this work exhibited a pH voltage sensitivity of 23.14 mV/pH, which is larger than those of the first ZnO pH sensor and CuO pH sensor but slightly lower than those of the second ZnO pH sensor and InN pH sensor. Besides, the pH detected range in our study was from 2 to 12, wider than the previous literature studies. While the pH sensitivity of nanorod and nanowire structures is not always superior to that of ZnGa_2O_4 thin films based on these literature studies, the nanorod and nanowire structures offer the advantage of increased surface contact area with the electrolyte. In the future, this will remain a research direction worthy of further exploration to enhance the performance of pH sensors.

CONCLUSIONS

In this study, we prepared different oxygen ratio ZnGa_2O_4 sensing films by an RF magnetron sputtering system. The ZnGa_2O_4 sensing films were analyzed by AFM and XRD, and they were connected with a commercial MOSFET to form an extended-gate field-effect transistor pH sensor. From the AFM analysis, it was observed that as the oxygen flow ratio increased, the higher surface roughness increased the sensing surface-to-volume ratio and further improved the response on the interface between the pH buffer solution and ZnGa_2O_4 sensing films. It could be found that the pH voltage sensitivity values with oxygen ratios of 0, 2, 4, and 6% were 8.71, 12.43, 16.29, and 23.14 mV/pH, respectively. The corresponding pH current sensitivity values with oxygen ratios of 0, 2, 4, and 6% were 5.41, 15.46, 22.22, and 33.49 $\mu\text{A}/\text{pH}$, respectively. Compared to fabricating with different oxygen ratios, the annealing treatment method could not improve the properties of the ZnGa_2O_4 extended-gate field-effect transistor pH sensor owing to a reduction in the surface site density, resulting in a poor reaction.

Table 1. pH Sensing Performance Comparison of Other Metal Oxide Materials

sensing film	method	structure	pH voltage sensitivity (mV/pH)	linearity	pH range	refs
ZnO	hydrothermal process	nanorod	15.4		4–12	35
ZnO	hydrothermal process	nanorod	24.67	0.986	4–10	36
InN	MBE	nanorod	22.66		4–10	37
CuO	thermal annealing of a Cu film at 450 °C for 5 h in air	nanowire	18.4		4–10	38
ZnGa ₂ O ₄	RF sputtering	film	23.14	0.921	2–12	this work

EXPERIMENTAL SECTION

The schematic structure of the ZnGa₂O₄ sensing films is depicted in Figure 8a. The fabrication process involved several

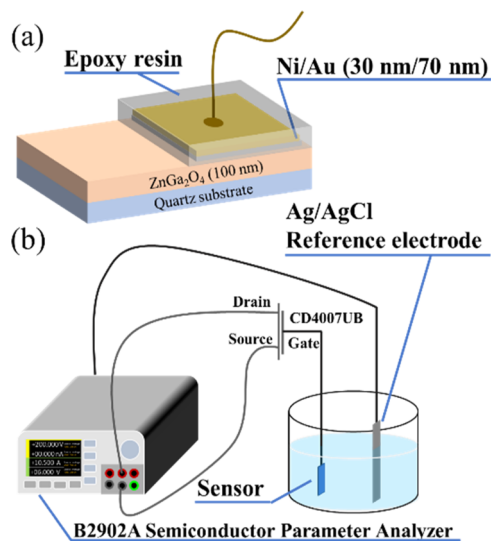


Figure 8. (a) Schematic structure of ZnGa₂O₄ sensing films. (b) Measurement system setup of the extended-gate field-effect transistor pH sensor with the ZnGa₂O₄ sensing films.

steps. First, quartz substrates were cleaned in an ultrasonic cleaning machine using a sequence of acetone, isopropyl alcohol, and deionized water, with each step lasting 5 min. Following the rinsing process, the substrates were dried using nitrogen gas. Next, ZnGa₂O₄ thin films were deposited using RF sputtering. The sputtering process was carried out with a fixed sputtering power of 80 W and a chamber pressure of 5 mTorr. The oxygen flow ratio within the sputtering chamber was varied to study its effect on the characteristics of the sensing films. Four oxygen flow ratios were examined, namely, 0, 2, 4, and 6%. Then, half of the ZnGa₂O₄ thin film was coated with Ni/Au (30/70 nm) by using an e-beam evaporator to serve as the contact electrode. Finally, a bonding wire was used to establish a connection between the bonding pad on the ZnGa₂O₄ thin film and the terminal of the MOSFET. The bonding pad was then encapsulated with epoxy resin to protect the metals from corrosion when exposed to the solution. The measurement setup, as depicted in Figure 8b, was employed to evaluate the performance of the ZnGa₂O₄ thin film. The setup involved the following components and steps. The ZnGa₂O₄ sensing films and Ag/AgCl reference electrodes were immersed in a buffer solution. The ZnGa₂O₄ sensing films were connected to a commercial MOSFET (CD4007UBE) to serve as the gate of the EGFET pH sensors. The EGFET pH sensor was further connected to an Agilent B1500A semiconductor parameter analyzer and controlled using LabVIEW software. The EGFET pH sensors with different oxygen ratio

sensing films were measured, and the sensing sensitivity and linearity of the device were analyzed in the pH range of 2–12.

AUTHOR INFORMATION

Corresponding Author

Sheng-Po Chang – Department of Microelectronics Engineering, National Kaohsiung University of Science and Technology, Kaohsiung City 88157, Taiwan; orcid.org/0000-0002-4126-0576; Phone: +886-919-745363; Email: changsp@nkust.edu.tw

Authors

Chia-Hsun Chen – Institute of Electro-Optical and Material Science, National Formosa University, Yunlin 632301, Taiwan

Shu-Bai Liu – Department of Electronic Engineering, National Kaohsiung University of Science and Technology, Kaohsiung City 80778, Taiwan

Complete contact information is available at:

<https://pubs.acs.org/10.1021/acsomega.3c09965>

Author Contributions

†C.H.C., S.B.L., and S.P.C. contributed equally to this work. C.H.C. wrote the paper.

Notes

The authors declare no competing financial interest.

ACKNOWLEDGMENTS

This work was supported by the Ministry of Science and Technology under contract number, 111-2222-E-273-001-MY2, 111-2221-E-006-030-MY3, NSTC 111-2222-E-150-003-MY2, and 111-2515-S-273-001.

REFERENCES

- Ren, H.; Liang, K.; Li, D.; Chen, Y.; Tang, Y.; Wang, Y.; Li, F.; Liu, G.; Zhu, B. Field-effect transistor-based biosensor for pH sensing and mapping. *Adv. Sens. Res.* **2023**, *2*, No. 2200098, DOI: [10.1002/adrs.202200098](https://doi.org/10.1002/adrs.202200098).
- Tang, Y.; Zhong, L.; Wang, W.; He, Y.; Han, T.; Xu, L.; Mo, X.; Liu, Z.; Ma, Y.; Bao, Y.; Gan, S.; Niu, L. Recent Advances in Wearable Potentiometric pH Sensors. *Membranes* **2022**, *12*, No. 504, DOI: [10.3390/membranes12050504](https://doi.org/10.3390/membranes12050504).
- Palit, S.; Her, J. L.; Pang, S. T.; Pan, T. M. Effect of silver doping on sol-gel synthesized RuAgxOy-based extended-gate field-effect transistor flexible sensor device. *Sens. Actuators, A* **2023**, *357*, No. 114392, DOI: [10.1016/j.sna.2023.114392](https://doi.org/10.1016/j.sna.2023.114392).
- Yao, H.; Shum, A. J.; Cowan, M.; Lähdesmäki, I.; Parviz, B. A. A contact lens with embedded sensor for monitoring tear glucose level. *Biosens. Bioelectron.* **2011**, *26* (7), 3290–3296.
- Ratanaporncharoen, C.; Tabata, M.; Kitasako, Y.; Ikeda, M.; Goda, T.; Matsumoto, A.; Tagami, J.; Miyahara, Y. pH mapping on tooth surfaces for quantitative caries diagnosis using micro Ir/IrOx pH sensor. *Anal. Chem.* **2018**, *90* (7), 4925–4931.
- Millward, A.; Shaw, L.; Harrington, E.; Smith, A. J. Continuous monitoring of salivary flow rate and pH at the surface of the dentition

- following consumption of acidic beverages. *Caries Res.* **1997**, *31* (1), 44–49.
- (7) Zhang, J.; Zhao, D.; Yang, H.; Li, C.; Si, H.; Wu, D. Dual-mechanism model to describe the slow response of ISFETs. *IEEE Sens. J.* **2019**, *19* (17), 7471–7478.
- (8) Si, H.; Pan, N.; Zhang, X.; Liao, J.; Rumyantseva, M. N.; Gaskov, A. M.; Lin, S. A real-time on-line photoelectrochemical sensor toward chemical oxygen demand determination based on field-effect transistor using an extended gate with 3D TiO₂ nanotube arrays. *Sens. Actuators, B* **2019**, *289* (15), 106–113.
- (9) Young, S. J.; Lai, L. T.; Tang, W. L. Improving the performance of pH sensors With one-dimensional ZnO nanostructures. *IEEE Sens. J.* **2019**, *19* (23), 10972–10976.
- (10) Shen, Y. S.; Wang, W. K.; Horng, R. H. Characterizations of metal-oxide-semiconductor field-effect transistors of ZnGaO grown on sapphire substrate. *IEEE J. Electron Devices Soc.* **2017**, *5* (2), 112–116.
- (11) Lin, Y. H.; Lee, C. T. Stability of Indium Gallium Zinc Aluminum Oxide Thin-Film Transistors with Treatment Processes. *J. Electron. Mater.* **2017**, *46* (2), 936–940.
- (12) Wu, Y.; Fu, X.; Zhang, K.; Tao, Z.; Fan, Y.; Lu, W. A strategy of high-sensitivity solar-blind photodetector for fabricating graphene surface modification ZnGa₂O₄/Ga₂O₃ core-shell structure nanowire networks. *Ceram. Int.* **2023**, *49* (11), 18248–18254, DOI: 10.1016/j.ceramint.2023.02.196.
- (13) Li, L.; Hu, Z.; Kang, Y.; Cao, S.; Xu, L.; Yu, L.; Zhang, L.; Yu, J. C. Electrochemical generation of hydrogen peroxide from a zinc gallium oxide anode with dual active sites. *Nat. Commun.* **2023**, *14*, No. 1890, DOI: 10.1038/s41467-023-37007-9.
- (14) Liu, B. D.; Su, Y. K.; Chen, S. C. Ion-sensitive field-effect transistor with silicon nitride gate for pH sensing. *Int. J. Electron. Theor. Exp.* **1989**, *67* (1), 59–63.
- (15) Bergveld, P. Development of an Ion-Sensitive Solid-State Device for Neurophysiological. *IEEE Trans. Biomed. Eng.* **1970**, *BME-17*, 70–71.
- (16) Bausells, J.; Carrabina, J.; Errachid, A.; Merlos, A. Ion-sensitive field-effect transistors fabricated in a commercial CMOS technology. *Sens. Actuators, B* **1999**, *57* (1), 56–62.
- (17) van der Spiegel, J.; Lauks, I.; Chan, P.; Babic, D. The extended gate chemically sensitive field effect transistor as multi-species microprobe. *Sens. Actuators* **1983**, *4*, 291–298.
- (18) Mazzara, F.; Patella, B.; Agostino, C. D.; Bruno, M. G.; Carbone, S.; Lopresti, F.; Aiello, G.; Torino, C.; Vilasi, A.; Riordan, A. O.; Inguanta, R. PANI-based wearable electrochemical sensor for pH sweat monitoring. *Chemosensors* **2021**, *9* (7), No. 169, DOI: 10.3390/chemosensors9070169.
- (19) García-Guzmán, J. J.; Rafols, C. P.; Cuartero, M.; Crespo, G. A. Toward in vivo transdermal pH sensing with a validated microneedle membrane electrode. *ACS Sens.* **2021**, *6* (3), 1129–1137.
- (20) Kashaninejad, N.; Munaz, A.; Moghadas, H.; Yadav, S.; Umer, M.; Nguyen, N. T. Microneedle arrays for sampling and sensing skin interstitial fluid. *Chemosensors* **2021**, *9* (4), No. 83, DOI: 10.3390/chemosensors9040083.
- (21) Ecken, H.; Ingebrandt, S.; Krause, M.; Richter, D.; Hara, M.; Offenhäuser, A. 64-channel extended gate electrode arrays for extracellular signal recording. *Electrochim. Acta* **2003**, *48* (20), 3355–3362.
- (22) Chiang, J. L.; Chiang, J. L. *Study on the Characterizations and Applications of the pH-Sensor with GZO/Glass Extended-Gate FET*, IEEE 5th International Nanoelectronics Conference (INEC); IEEE, 2013.
- (23) Pullano, S. A.; Tasneem, N. T.; Mahbub, I.; Shamsir, S.; Greco, M.; Islam, S. K.; Fiorillo, A. S. Deep submicron EGFET based on transistor association technique for chemical sensing. *Sensors* **2019**, *19* (5), No. 1063, DOI: 10.3390/s19051063.
- (24) Slewa, L. H.; Abbas, T. A.; Ahmed, N. M. Effect of Sn doping and annealing on the morphology, structural, optical, and electrical properties of 3D (micro/nano) V₂O₅ sphere for high sensitivity pH-EGFET sensor. *Sens. Actuators, B* **2020**, *305* (15), No. 127515, DOI: 10.1016/j.snb.2019.127515.
- (25) Chae, M. S.; Park, J. H.; Son, H. W.; Hwang, K. S.; Kim, T. G. IGZO-based electrolyte-gated field-effect transistor for in situ biological sensing platform. *Sens. Actuators, B* **2018**, *262* (1), 876–883.
- (26) Yang, C. C.; Chen, K. Y.; Su, Y. K. TiO₂ nano flowers based EGFET sensor for pH sensing. *Coating* **2019**, *9* (4), No. 251, DOI: 10.3390/coatings9040251.
- (27) Ghoneim, M. T.; Nguyen, A.; Dereje, N.; Huang, J.; Moore, G. C.; Murzynowski, P. J.; Dagdeviren, C. Recent progress in electrochemical pH-sensing materials and configurations for biomedical applications. *Chem. Rev.* **2019**, *119* (8), 5248–5297.
- (28) Batista, P. D.; Mulato, M. ZnO extended-gate field-effect transistors as pH sensors. *Appl. Phys. Lett.* **2005**, *87* (14), No. 143508, DOI: 10.1063/1.2084319.
- (29) Wu, Y. C.; Wu, S. J.; Lin, C. H. High performance EGFET-based pH sensor utilizing low-cost industrial-grade touch panel film as the gate structure. *IEEE Sens. J.* **2015**, *15* (11), 6279–6286.
- (30) Tsai, Y. T.; Chang, S. J.; Ji, L. W.; Hsiao, Y. J.; Tang, I. T. Fast detection and flexible microfluidic pH sensors based on Al-doped ZnO nanosheets with a novel morphology. *ACS Omega* **2019**, *4* (22), 19847–19855.
- (31) Varghese, A.; Chinnamuthan, P.; Bhargava, L. Fabrication and pH-sensitivity analysis of MOS-HEMT dimensional variants for bio-sensing applications. *IEEE Trans. NanoBiosci.* **2021**, *20* (1), 28–34.
- (32) Singh, A. K.; Yen, C. C.; Wu, D. S. Structural and photodetector characteristics of Zn and Al incorporated ZnGa₂O₄ films via co-sputtering. *Results Phys.* **2022**, *33*, No. 105206, DOI: 10.1016/j.rinp.2022.105206.
- (33) Cha, J. H.; Kim, K. H.; Park, Y. S.; Park, S. J.; Choi, H. W. Photoluminescence characteristics of nanocrystalline ZnGa₂O₄ phosphors obtained at different sintering temperatures. *Mol. Cryst. Liq. Cryst.* **2009**, *499* (1), 85–91.
- (34) Chang, S. P.; Huang, W. L.; Huang, L. W.; Pan, S. Y.; Lai, W. C.; Chang, S. J. Tri-Layer structure ZnGa₂O₄-based resistive random access memory. *ECS J. Solid State Sci. Technol.* **2021**, *10*, No. 065003, DOI: 10.1149/2162-8777/ac04fd.
- (35) Van Thanh, P.; Nhu, L. T. Q.; Mai, H. H.; Tuyen, N. V.; Doanh, S. C.; Viet, N. C.; Kien, D. T. Zinc oxide nanorods grown on printed circuit board for extended-gate field-effect transistor pH sensor. *J. Electron. Mater.* **2017**, *46*, 3732–3737.
- (36) Young, S. J.; Chu, Y. J.; Chen, Y.-L. Enhancing pH sensors performance of ZnO nanorods with Au nanoparticles adsorption. *IEEE Sens. J.* **2021**, *21* (12), 13068–13073.
- (37) Chen, S. X.; Chang, S. P.; Chang, S. J. Investigation of InN nanorod-based EGFET pH sensors fabricated on quartz substrate. *Dig. J. Nanomater. Biostructures* **2014**, *9* (4), 1505–1511.
- (38) Chang, S. P.; Yang, T. H. Sensing performance of EGFET pH sensors with CuO nanowires fabricated on glass substrate. *Int. J. Electrochem. Sci.* **2012**, *7* (6), 5020–5027.